Solid-State NMR Spectra and Long Intradimer Bonds in the π-$[TCNE]_2^{2-}$ Dianion

Mark Strohmeier, Dewey H. Barich, David M. Grant,* Joel S. Miller, Ronald J. Pugmire, and Jack Simons

Department of Chemistry, University of Utah, 315 South 1400 East, Room 2020, Salt Lake City, Utah 84112-0850

Received: March 28, 2006

The principal ^{13}C chemical-shift values for the π-$[TCNE]_2^{2-}$ dimer anion within an array of counterions have been measured to understand better the electronic structure of these atypical chemical species in several related TCNE-based structures. The structure of π-$[TCNE]_2^{2-}$ is unusual as it contains two very long C−C bond lengths (ca. 2.9 Å) between the two monomeric units and has been found to exist as a singlet state, suggestive of a $^1A_{1g}$ ($b_{2u}^2b_{1g}^0$) electronic configuration. A systematic study of several oxidation states of $[TCNE]^n$ ($n = 0, 1-, 2-$) was conducted to determine how the NMR chemical-shift tensor values change as a function of electronic structure and to understand the interactions that lead to spin-pairing of the monomer units. The density functional theory (DFT) calculated nuclear shielding tensors are correlated with the experimentally determined principal chemical-shift values. Such theoretical methods provide information on the tensor magnitudes and orientations of their principal tensor components with respect to the molecular frame. Both theoretical and experimental ethylenic chemical-shielding tensors reveal high sensitivity in the component, $\delta_\perp$, lying in the monomer molecular plane and perpendicular to the π-electron plane. This largest shift dependence on charge density is observed to be about −111 ppm/e^- for $\delta_\perp$. The component in the molecular plane but parallel to the central C═C bond, $\delta_\parallel$, exhibits a sensitivity of approximately −43 ppm/e^-. However, the out-of-plane component $\delta'_\perp$ shows a minimal dependence of −2.6 ppm/e^- on the oxidation state (n) of $[TCNE]^n$. These relative values support the claim that it is changes within the ethylenic π-electrons and not the σ-electrons that best account for the dramatic variations in bonding and shift tensors in this series of compounds. Concerning the intraion bonding, relatively weak Wiberg bond orders between the two monomeric components of the dimer correlate with the long bonds linking the two $[TCNE^\bullet]^-$ monomers. The chemical-shift tensors for the cyano group, compared to the ethylene shifts, exhibit a reduced sensitivity on the TCNE oxidation state. The experimental principal chemical-shift components agree (within typical errors) with the calculated quantum mechanical shieldings used to correlate the bonding. The embedded ion model (EIM) was used to investigate the typically large electrostatic lattice potential in these ionic materials. Chemical-shielding principal values calculated with the EIM model differ from experiment by ±3.82 ppm on average, whereas in the absence of an electrostatic field model, the experimental and theoretical results agree by ±4.42 ppm, which is only a modest increase in error considering the overall ionic magnitudes associated with the tensor variations. Apparently, the effects of the sizable long-range electrostatic fields cancel when the shifts are computed because of lattice symmetry.

Introduction

TCNE, π-$[TCNE]_2^{2-}$, and $[TCNE]^{2-}$ correspond to a series of relatively stable oxidation states that may be isolated and studied by a variety of methods[1] including solid-state NMR (SSNMR). The 1− oxidation state of the tetracyanoethylene series can arise from either the paramagnetic monomer, $[TCNE]^{\bullet-}$, or the diamagnetic dimer, π-$[TCNE]_2^{2-}$. The monomer, which is a doublet state, yields a paramagnetic sample that would be unobservable by NMR due to line broadening from the free unpaired electrons. The species with the second 1− oxidation state is a dimer, π-$[TCNE]_2^{2-}$, which is a singlet with the term symbol assigned to $^1A_{1g}$ ($b_{2u}^2b_{1g}^0$) symmetry.[2,3] The observed long C−C bonds in π-$[TCNE]_2^{2-}$ have been further supported through the measurement of characteristic IR and UV/visible absorptions, and as a consequence of the long 4-center bond, spin-pairing is also observed for π-$[TCNE]_2^{2-}$. None of the samples indicate the presence of a paramagnetic free radical $[TCNE]^{\bullet-}$ monomer except for a small doublet impurity.[2] Moreover, crystal structures have been determined and confirm the structures for TCNE,[4] $[NEt_4^+]_2[TCNE]_2^{2-}$,[5] $[TDAE]^{2+}$-$[TCNE]_2^{2-}$,[6] and $[TDAE]^{2+}[TCNE]^{2-}$.[7] Finally, solid-state NMR chemical shift tensors support the interpretations offered by quantum mechanical computations in this series of materials. $[TDAE]^{2+}$ is the tetrakis(dimethylamino)ethylene dication.

To probe the nature and strength of the intradimer bonding in π-$[TCNE]_2^{2-}$ three theoretical studies have been carried out.[2,8,9] In these studies attempts have been made to isolate and identify the contributions of various effects to the bonding, including the following: (i) the Coulomb repulsion between the two anionic centers that tends to disfavor bonding; (ii) the effects of surrounding countercations that tend to cancel the anions' Coulomb repulsions; (iii) the singlet coupling of the two unpaired electrons of the monomer anions that would arise if a covalent bond is formed; and (iv) the van der Waals (dispersion) interaction that is also always present and that tends to bind the two anionic fragments together. As with all bond-

10.1021/jp061920s CCC: $33.50
Published on Web 06/06/2006

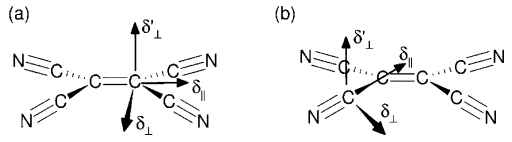

Figure 1. Orientation of the ^{13}C chemical-shift tensor with respect to the molecular frame. (a) Ethylenic carbon ($C_{ethylenic}$) shift tensor orientation. Neutral TCNE is planar. However, in π-$[TCNE]_2^{2-}$ structures the cyanide groups are bent out of the nominal molecular plane by several degrees. Nevertheless, the overall molecular geometry at the ethylenic carbon can still be approximated as being planar and the nomenclature of in-plane and perpendicular components is used for all compounds for the sake of simplicity. (b) Cyano carbon (C_{cyano}) shift tensor orientation. Note that the remainder of the TCNE molecule breaks the local axial symmetry of the cyano group.

forming events, the combination of all attractive forces (e.g, van der Waals and covalent bonding) and all repulsive forces (e.g., Coulomb and inner-shell valence/Pauli repulsion), when brought into balance, determines whether a minimum on the potential energy surface will or will not exist. For π-$[TCNE]_2^{2-}$ these various contributions have been shown to produce net attraction but only when dispersion and covalent bonding are treated and when the interanion Coulomb repulsion is compensated by the effects of surrounding counterions.[2,8,9] Theoretical work also suggested that in the absence of any stabilization by nearby cations or by solvent stabilization there is no minimum on the π-$[TCNE]_2^{2-}$ potential surface. However, when counterions or strong solvation effects are present, theory has shown that a minimum (near 3 Å) arises on this surface.[2,8,9]

It is worth noting that the equilibrium distance (ca. 2.9 Å) found in the crystal structures is well below the carbon−carbon van der Waals distance of about 3.4 Å for closed shell molecules.[10] This unusually large decrease may be explained[11,12] by an offsetting of the Pauli repulsion induced by significant covalent spin-pairing of the electrons.

Using shielding tensors one can characterize both electronic and molecular structural features that are independent of other spectroscopic and theoretical methods. The theory of the NMR chemical-shielding is well understood and both ab initio and DFT methods correlate the corresponding experimental chemical-shift parameters with structure, conformation, bonding, and other molecular properties for a variety of organic, inorganic, and biochemical compounds.[13−16] Many ^{13}C principal chemical-shift components have been experimentally determined and constitute a formidable database to establish these trends.[17] Several ^{13}C studies have investigated the effect of changes in π-bonds on olefinic and aromatic principal chemical-shift values, and general rules have been formulated for discussing these systems.[18−20] In-plane ^{13}C chemical-shift tensor components for aromatic or olefinic hydrocarbons in the region of the ethylenic bond and neighboring atoms exhibit an extensive sensitivity to π-electrons and the paramagnetic shielding spans more than a hundred ppm. These sizable shift variations arise from the magnetic field mixing of π- and σ*-orbitals or σ- and π*-orbitals. The magnitude of the tensor shifts is proportional to the promotional energy, $1/\Delta E$, as proposed by Ramsey.[21] The nomenclature and the orientation of the principal components used throughout this publication are illustrated in Figure 1.

The presence of narrow NMR signals supports the existence of a diamagnetic dimer in contrast to the paramagnetic monomer, which would introduce very strong spin−spin interactions between the free electrons and the carbon nuclei with broadening and shifting of the NMR signal beyond detection limits.[22,23] This observation suggests that the long π-bond pairs the two electrons in the overlapping π*-orbitals between the interacting components of the dimer. This conclusion agrees with that of Miller and co-workers,[2] using magnetic susceptibility and ESR to confirm the singlet state for the π-$[TCNE]_2^{2-}$ dimer species.

Typically, large variations in the shift tensors are observed whenever the structural differences are related to strong interactions (e.g., large energy gradients and large $1/\Delta E$ terms in the paramagnetic shielding expression).[21] For example, chemical-shift vs bond-length gradients of 300 ppm/Å are noted for the π-double bonds in acenaphthene.[24,25] In σ-single bonds shift gradients of up to 76 ppm/Å have been reported. Furthermore, ^{13}C shift tensor variations in methyl groups have been correlated with nonbonding, van der Waals interactions between the attached hydrogen atoms.[29,30]

The shielding gradient as a function of dimer distance for the most sensitive $\delta_\perp$ component is only 7.49 ppm/Å, while the corresponding gradients for $\delta'_\perp$ and $\delta_\parallel$ are essentially negligible in $[TCNE]_2^{2-}$. These small gradients are 1 to 2 orders of magnitude smaller than those observed for typical single bonds.

Wave function energies, chemical shift tensors, and X-ray diffraction structures reflect a variety of physical properties, some related to lattice parameters more than others. Nonetheless, wave functions and chemical shieldings depend on similar energy considerations and both exhibit similar reliance on molecular motions. Conversely, the X-ray diffraction structural parameters arise from linear lattice displacements. Further, lattice parameters are dissimilar from average values arising from molecular motion. Fortunately, the average structure of π-$[TCNE]_2^{2-}$, involving very weak and longer bonds, is still sensitive to the intradimer bond length of 2.9 Å obtained from X-ray diffraction. Chemical-shift tensors have been shown to depend also on valence and conformational angles. Shielding parameters are also sensitive to intra- and intermolecular effects arising from hydrogen bonding, nonbonding repulsions, and electrostatic field interactions.[26−30]

Methods

X-ray Diffraction. While the positions of the heavy atoms are readily obtained from the X-ray data, proton locations are less certain especially in microcrystalline powder samples. The less accurate hydrogen atom positions in the cations were optimized by using the B3LYP/D95* level of theory.

Solid-State ^{13}C NMR. Data were collected on a CMX-400 NMR spectrometer operating at 400.12 MHz for ^1H and at 100.62 MHz for ^{13}C. All spectra are referenced relative to TMS via a secondary external reference to the high-frequency peak of adamantane at 38.6 ppm. Air-sensitive samples were packed under a nitrogen atmosphere into 7.5 mm o.d. rotors made from zirconia. Dry nitrogen was used as the spinning gas to avoid sample contamination with air.

Because of the absence of protons in TCNE, direct excitation of the ^{13}C nuclei was used along with background suppression to eliminate a signal from the probe body.[31,32] TCNE has a ^{13}C longitudinal relaxation time (T_1) of nearly 15 min. Hence, a 15 min recycle delay was used to maximize signal-to-noise in a constant time experiment. The $\pi/2$ pulse width for ^{13}C was 4.0 μs. The total suppression of a sideband (TOSS)[33] spectrum was collected at a spinning speed of 4 kHz. The spinning speed was then lowered to 1850 Hz to collect a magic angle spinning (MAS) spectrum with a sufficient number of sidebands for accurate determination of the principal values of the chemical-shift tensors from the sideband patterns present in the spectrum. The spectral width was 55.249 kHz with 640 transients and 4096

TABLE 1: Parameters of FIREMAT Experiments[a]

	$[NEt_4^+]_2$-$[TCNE]_2^{2-}$	$[TDAE]^{2+}$-$[TCNE]^{2-}$	$[TDAE]^{2+}$-π-$[TCNE]_2^{2-}$
spinning speed/Hz	850	496	780
spectral window evolution/kHz	13.600	15.872	12.480
spectral window acquisition/kHz	81.600	95.232	74.880
transients	5568	480	5376
acquisition points	5568	4802	2978
increments	16	32	16

[a] ^{13}C π-pulse widths were 9.4−10.4 μs and ^1H $\pi/2$-pulse widths were 4.2−4.4 μs.

acquisition points for both spectra. The $\pi/2$ pulse width for ^1H was 4.4 μs and the ^{13}C π-pulses were 8.4 μs. Furthermore, two CP/MAS TOSS spectra with and without dipolar coupling were collected at a spinning speed of 4 kHz. A dephasing time of 42 μs was employed to eliminate CH_2 and CH peaks and to aid spectral assignment. A total of 256 transients, each of 2048 acquisition points and a spectral width of 50.0 kHz, were collected for each TOSS spectrum. The experimental parameters employed in slow-spinning FIREMAT[34] experiments are summarized for all samples in Table 1.

Data Analysis. Data were transferred to a Sun Enterprise 3500 and analyzed with software developed in-house. The C−N carbons, as well as some cationic carbons, are dipolar coupled to the quadrupolar ^{14}N nuclei in the sample. This coupling introduces second-order effects in the isotropic spectrum introducing errors into the TIGER processing.[35] Hence, the principal values for the ^{14}N coupled carbons were estimated from a fit of the 2D FID.[36] Individual sideband patterns were extracted for all uncoupled resonances with TIGER processing and were fitted subsequently to a shift tensor model.

Calculations. Quantum mechanical computations were performed with Gaussian-98 and Gaussian-03 software.[37] The shielding tensor calculations used gauge invariant atomic orbitals[38,39] (GIAO) at the B3LYP/D95** level of theory.[40−43] The theoretical shielding tensors were converted to the chemical-shift scale by using a linear fit of theory and experiment. The model compounds involved TCNE, π-$[TCNE]_2^{2-}$, $[TCNE]^{2-}$, acetonitrile, and ketenimine. A natural bond orbital (NBO) analysis was performed with use of NBO as implemented in Gaussian-03.[44] Accurate shift tensor computations were performed by using the heavy-atom positions obtained from diffraction data rather than from quantum chemical geometry optimization.

Results and Discussion

^{13}C Solid-State NMR Spectra. To understand the chemical-shift tensors in TCNE, π-$[TCNE]_2^{2-}$, and $[TCNE]^{2-}$ the spectra were determined for several different crystal structures. The values for the central ethylenic and cyano carbons are summarized in Tables 2 and 3. The existence of a NMR signal in Figure 2 for $[NEt_4^+]_2[TCNE]_2^{2-}$ indicates that the compounds are diamagnetic[2] in accord with the formation of the spin-paired valence electrons of the dimeric singlet π-$[TCNE]_2^{2-}$.

To discriminate the CH and CH_2 protonated carbon peaks of the cation from the ethylenic region of the spectra, dipolar dephased CP/MAS TOSS spectra of $[NEt_4^+]_2[TCNE]_2^{2-}$ were recorded. The dipolar-dephased experiment eliminates the methylene peak at 52.6 ppm in Figure 2. The ethylenic resonance of the anion at 58.5 ppm and the methyl peak at 7.7 ppm are retained. The cyano carbons are absent in the spectra presumably because of the strong nitrogen dipolar coupling

TABLE 2: Ethylenic Carbon Chemical-Shift Data[a]

compd	$\delta_\perp$	$\delta_\parallel$	$\delta'_\perp$	δ_{iso}	δ_{span}[b]	$\delta_{acentricity}$[c]
TCNE (neutral)	218	92	32	114	185	−33
$[NEt_4^+]_2[TCNE]_2^{2-}$	101	52	27	60	74	−12
$[NEt_4^+]_2[TCNE]_2^{2-}$	99	48	28	58	70	−16
$[TDAE]^{2+}[TCNE]_2^{2-}$	96	58	30	61	66	−5
$[TDAE]^{2+}[TCNE]_2^{2-}$	97	56	28	60	69	−7
$[TDAE]^{2+}[TCNE]^{2-}$	−6	10	26	10	32	0
$[TDAE]^{2+}[TCNE]^{2-}$	−13	8	23	6	36	3

[a] All values are in ppm from TMS. [b] $\delta_{span} = \delta_{11} - \delta_{33}$, when the principal values are ordered by $\delta_{11} > \delta_{22} > \delta_{33}$. [c] $\delta_{acentricity} = \delta_{22} - (\delta_{11} + \delta_{33})/2$, when the principal values are ordered by $\delta_{11} > \delta_{22} > \delta_{33}$.

TABLE 3: Cyano Carbon Chemical-Shift Data[a,b]

compd	$\delta_\perp$	$\mathbf{d}'_\perp$	$\delta_\parallel$	δ_{iso}	δ_{span}[c]	$\delta_{acentricity}$[d]
TCNE monoclinic	209	199	−80	109	288	135
TCNE monoclinic	209	199	−80	109	288	135
$[TDAE]^{2+}[TCNE]_2^{2-}$	228	204	−74	119	302	127
$[TDAE]^{2+}[TCNE]_2^{2-}$	228	201	−75	118	303	125
$[TDAE]^{2+}[TCNE]^{2-}$	238	224	−53	136	291	132
$[TDAE]^{2+}[TCNE]^{2-}$	236	218	−54	134	290	127

[a] All values are in ppm from TMS. [b] Principal shift values for the cyano carbon in $[NEt_4^+]_2[TCNE]_2^{2-}$ were not obtained, because of insufficient intensity of the resonances. [c] $\delta_{span} = \delta_{11} - \delta_{33}$, when the principal values are ordered by $\delta_{11} > \delta_{22} > \delta_{33}$. [d] $\delta_{acentricity} = \delta_{22} - (\delta_{11} + \delta_{33})/2$, when the principal values are ordered by $\delta_{11} > \delta_{22} > \delta_{33}$.

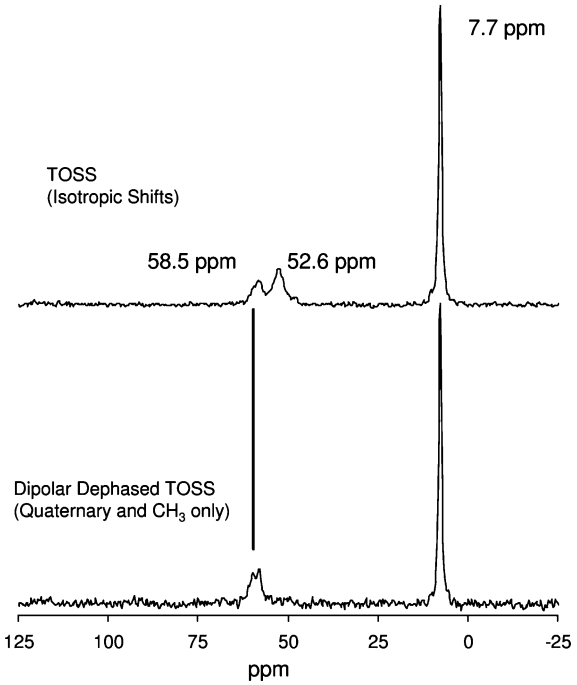

Figure 2. The top spectrum shows a standard CP/MAS spectrum of $[NEt_4^+]_2$ $[TCNE]_2^{2-}$ with a total suppression of sidebands (TOSS). The bottom spectrum used dipolar dephasing to eliminate peaks from CH_2 and CH carbons. The solid vertical line indicates the quaternary ethylenic carbon peak that is retained in the dipolar dephased spectrum. The peak at 52.6 ppm is assigned to the CH_2 carbons of the cation, since it is absent in the dipolar dephased spectrum.

(∼1.4 kHz) resulting in second-order line broadening and the wide sideband patterns. This leaves only a fraction of the intensity in the center-band that is observed in a TOSS spectrum. The spectrum of the neutral TCNE exhibits two sets of sidebands in Figure 3. The central carbon has an isotropic chemical shift, δ_{iso}, of 114 ppm. The cyano carbon peak at 109 ppm exhibits

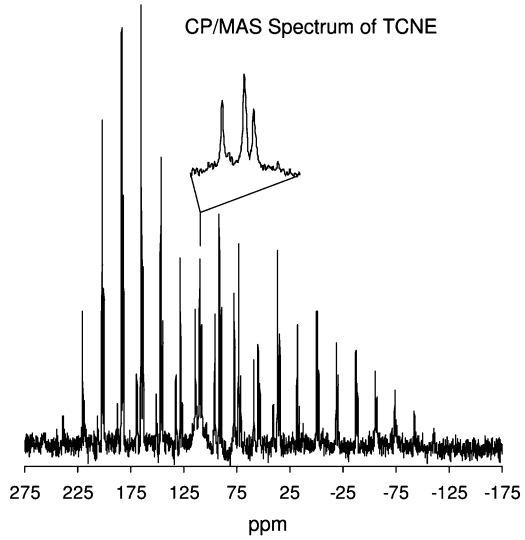

Figure 3. ^{13}C CP/MAS spectrum of TCNE with a spinning speed of 1850 Hz. The inset shows the center bands of the two sideband pattern. The left one (114 ppm) is the central carbon of the TCNE, while the right two peaks (centered at 109 ppm) exhibit the 2:1 splitting of the CN carbons due to the coupling to the adjacent ^{14}N. The larger area for the CN carbons is due to the presence of two CN carbons for each central carbon. The monoclinic crystal form of TCNE has two distinct CN carbons in the crystal structure, but they are degenerate in the NMR spectrum.

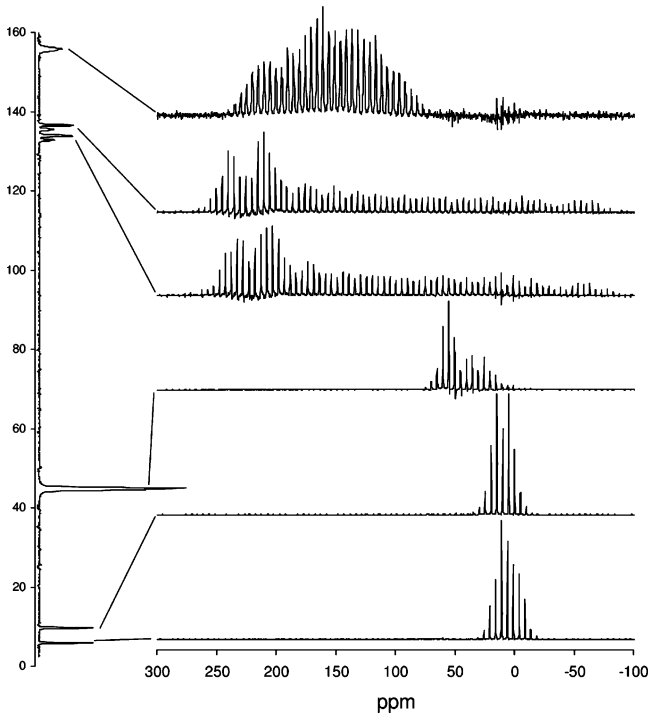

Figure 4. ^{13}C FIREMAT spectrum of $[TDAE]^{2+}[TCNE]^{2-}$. On the left is the guide spectrum, the isotropic-only spectrum derived from the FIREMAT data set. To the right are the individual sideband patterns associated with each isotropic peak. The two bottom sideband patterns are those associated with the ethylenic carbons of the $[TCNE]^{2-}$ anion.

the characteristic splitting of the $^{13}C-^{14}N$ coupling as shown in the inset of Figure 3.[36]

FIREMAT experiments were acquired for $[TDAE]^{2+}$-$[TCNE]_2^{2-}$, $[NEt_4^+]_2[TCNE]_2^{2-}$, and $[TDAE]^{2+}[TCNE]^{2-}$ to obtain chemical-shift tensor principal values. The $[TDAE]^{2+}$-$[TCNE]^{2-}$ FIREMAT spectrum given in Figure 4 is discussed as an example. The isotropic guide spectrum exhibits six peaks on the left-hand side of Figure 4. The corresponding sideband patterns for each isotropic resonance, which were extracted with TIGER processing, are shown on the right-hand side.[34] The isotropic peaks at 45 and 156 ppm can be assigned to the $[TDAE]^{2+}$ methyl and ethylenic carbon positions, respectively. Both resonances are considerably broadened by the dipolar coupling to the neighboring ^{14}N quadrupole. The two crystallographic positions for the ethylenic carbon and the cyano carbon of the $[TCNE]_2^{2-}$ dimer are resolved at 8 ± 2 and 135 ± 1 ppm, respectively. The cyano carbon resonances reveal the distinctive two-to-one doublet structure of dipolar coupling between ^{13}C and ^{14}N. This second-order effect complicates somewhat the application of TIGER processing of these resonances. Nevertheless, TIGER sideband patterns for these resonances provide approximate solutions.

Ethylenic ^{13}C Shift Tensors. Electron reduction of TCNE to π-$[TCNE]_2^{2-}$ and to $[TCNE]^{2-}$ has a profound effect on the principal shift values of the central carbons. The orientation of the principal shift values in planar π-bonded systems, such as planar aromatic hydrocarbons and olefins, is proscribed by the local symmetry of the ^{13}C.[18-20] This local symmetry requires that principal components be oriented perpendicular to a molecular plane, as depicted in Figure 1. The π-$[TCNE]_2^{2-}$ deviate very slightly from planarity by a few degrees, hence, the dihedral angles observed in the crystal structures are rather small. The local symmetry of the dimer is assumed to be planar for the sake of simplicity. The terminal cyano groups in $[TCNE]^{2-}$ are twisted by 90° about the central ethylenic bond; however, local planar symmetry of the two sp^2 ethylenic carbons is retained. This configuration leaves the middle C−C bond as an essentially single σ-bond.

The experimental and theoretical principal shift components for the central carbons in TCNE, π-$[TCNE]_2^{2-}$, and $[TCNE]^{2-}$ are described in Figure 5. The assignment of the principal components to $\delta'_\perp$, $\delta_\perp$, and $\delta_\parallel$ is supported by excellent agreement between the experimental and theoretical shift tensors. Since only electronic currents perpendicular to a principal component contribute to the shift magnitude, the principal shift components represent a very sensitive spatially resolved description of the 3D electronic structure.[45] Thus, the $\delta'_\perp$ component is affected only by electron currents in the local sp^2 molecular plane, i.e., electrons that are located in the σ-bonds. As observed, this component is expected to be relatively insensitive to the oxidation state of TCNE as the σ-electrons are much less readily polarized. The in-plane components $\delta_\perp$ and $\delta_\parallel$ of the shift tensor mainly arise from paramagnetic orbital contributions and result from magnetic-field mixing of excited-state and ground-state wave functions that are connected by dipolar allowed transitions.[46] π-Electron orbitals are influenced most by close atoms. Ramsey[21] discussed orbital paramagnetism using perturbation theory. The differences in occupancy of the weak π-bonds or low-lying π^* orbitals has a profound effect on the paramagnetic electron currents. Consequently, a dramatic effect on the in-plane shift components is observed upon charge reduction.

The overall agreement in Figure 5 between experimental and calculated principal shift values is somewhat surprising considering the very large shift variations encountered in this study. The electronic structure must change appreciably to account for the magnitude of these structural and shielding variations. The experimentally observed shift in $\delta_\perp$ and $\delta_\parallel$ upon reduction is -111 ppm/e^- and -43 ppm/e^-, respectively. This is in good agreement with the DFT calculations that yield respective shifts of -115 ppm/e^- for $\delta_\perp$ and -38 ppm/e^- for $\delta_\parallel$. Conversely, the theory and experimental values for $\delta'_\perp$ show a minimal dependence of -2.6 and -0.72 ppm/e^- for the experimental

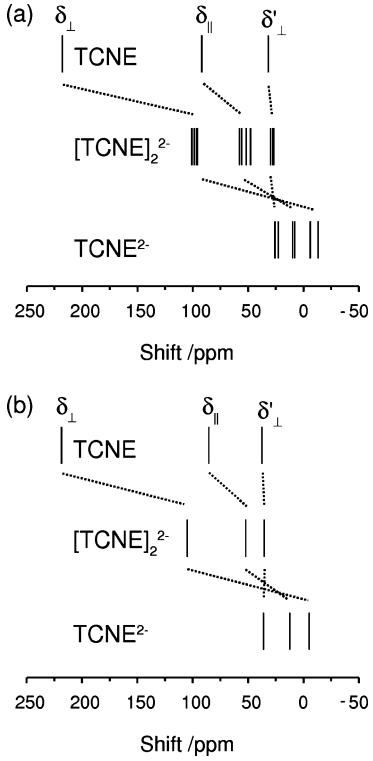

Figure 5. (a) Experimental and (b) theoretical ethlylenic ^{13}C principal shift components of TCNE oxidation states. Geometries of TCNE and $[TCNE]^{2-}$ were fully geometry optimized prior to shielding calculations. The intradimer distance in π-$[TCNE]_2^{2-}$ was fixed at 2.9 Å and all other parameters were geometry optimized. The calculated nuclear shielding values were converted to the chemical-shift scale by using an isotropic shift of 198 ppm for the bare nucleus and a scaling factor of -1.02.

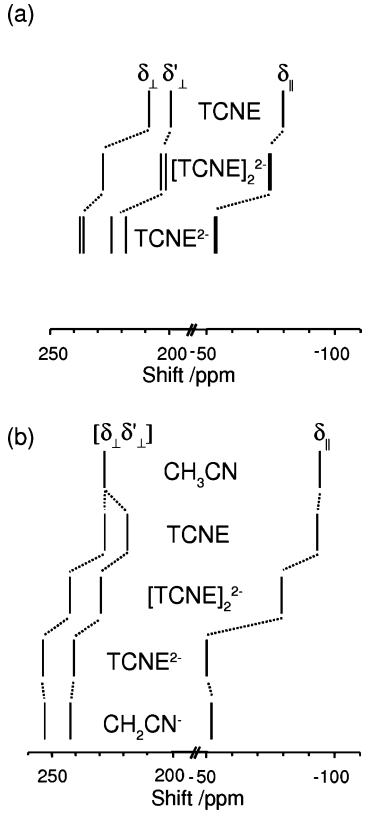

Figure 6. (a) Experimental and (b) theoretical cyano ^{13}C principal shift components of TCNE oxidation states and related acetonitrile and ketenimine. The monomer distance in π-$[TCNE]_2^{2-}$ was fixed at 2.9 Å and all other parameters were geometry optimized. The calculated nuclear shielding values were converted to the chemical-shift scale by using an isotropic shift of 198.0 ppm for the bare nucleus and a scaling factor of -1.03.

and theoretical values, respectively. The span of the shift tensor is reduced appreciably going from TCNE to $[TCNE]^{2-}$ as a result of quenching the π-orbital momentum with the corresponding consequence upon the paramagnetic shielding. Similar effects have been reported in the principal shift components in olefins and their metal complexes where the population of the π*-orbital is altered by back-bonding from the metal center to the olefin.[14,16]

Cyano ^{13}C Shift Tensors. Successive electron oxidation of $[TCNE]^{2-}$ to π-$[TCNE]_2^{2-}$ and then to TCNE also affects the principal shift values of the cyano carbons, although by a lesser amount than noted in the ethylene carbons. The 3-fold symmetry of an idealized cyano group in acetonitrile requires one of the principal axes of the chemical-shift tensor to be parallel and the remaining two degenerate axes perpendicular to the CN bond as depicted in Figure 1. Since the remaining TCNE molecular fragments break the axial symmetry of the CN bond, the two perpendicular orientations may be distinguished where $\delta'_\perp$ is assigned respectively to the orientation perpendicular to the TCNE molecular plane and $\delta_\perp$ to the orientation in the molecular plane (see Figure 1). In an idealized triply bonded CN group, the paramagnetic shielding contributions quench for the orientation parallel to the CN bond, leaving only the diamagnetic shielding to determine the principal shift component $\delta_\parallel$ along this direction. When a group with lower molecular symmetry is bonded to the cyano group the local axial symmetry is broken and consequently the two perpendicular components become distinguishable and modest paramagnetic contributions are introduced in $\delta_\parallel$. This shifts $\delta_\parallel$ to higher frequencies and results in nondegenerate perpendicular components $\delta'_\perp$ and $\delta_\perp$.[47] Larger effects are observed when the groups conjugate with the cyano π-electrons.[19,48]

The principal shift components of the cyano group indicate the different degrees of electron delocalization in the different TCNE oxidation states. The experimental and theoretical chemical-shift components of the model compounds are summarized in Figure 6. Here the shifts of acetonitrile and ketenimine serve as simplified limiting examples of the electronic structure of the cyano groups in TCNE. The quantitative agreement between model calculations and experimental values is remarkably outstanding. Geometry optimization of the X-ray structure affects the cyano $\delta'_\perp$ and $\delta_\perp$ shift tensor components; and the theoretical trends are preserved in Figure 6. This agreement reveals that the largest variation in the three TCNE species is observed in the $\delta_\parallel$ component of the cyano tensor shifts. The $\delta_\parallel$ component shifts to higher frequencies due to the diamagnetic shielding, as discussed above. Both the experimental shift components and the theoretical model follow the same trends. The paramagnetic shielding of the $\delta_\parallel$ component upon electronic oxidation may be attributed to the reduced population of the molecular orbital of the $C_{ethylenic}-C_{cyano}$ π-bond character and C≡N antibonding character. Population of this orbital delocalizes some of the additional electronic charge from the ethylenic carbons into the four cyano nitrogen atoms. This situation is comparable to ketenimine where the cyano carbon in $[TCNE]^{2-}$ has similar theoretical principal components to those found experimentally.

EIM Calculations. The quantum mechanical embedded ion method (EIM) optimizes the crystal's atomic charges within the charge array specified by the diffraction data. The EIM[49] initially

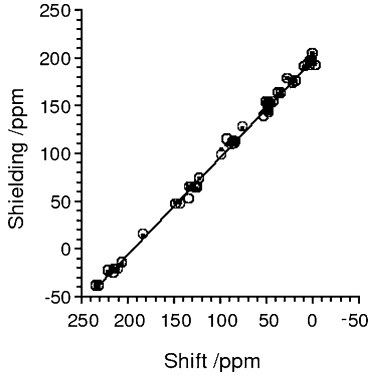

Figure 7. Calculated nuclear shieldings vs measured chemical-shift tensors in the icosahedral representation. The solid circles represent the NMR chemical shielding tensor values calculated with the EIM. The solid line is the best fit to these values and has a slope of −1.02 and an intercept of 198 ppm. The open circles represent the calculated values from the oversimplified models of isolated molecules or anions.

employs point charges obtained from a natural population analysis[50,51] (NPA). The method iterates the calculated point charges by using the theoretical approach of Ewald.[52] This method optimizes the position and electrostatic charges of the hydrogen atoms while adjusting the charges on the heavy atoms for the positions obtained for the diffraction data. These data reproduce the Madelung constant associated with the electrostatic potential and yield an array of partial atomic charges that are located at crystallographic nuclear positions. The EIM self-consistent potential accounts for polarization and electrostatic lattice effects. This method has been shown to reproduce reliably the chemical-shift tensors of several ionic and hydrogen bonded species.[53−56]

The DFT Kohn−Sham orbitals and shielding tensors for TCNE, $[NEt_4^+]_2[TCNE]_2^{2-}$, $[TDAE]^{2+}[TCNE]_2^{2-}$, and $[TDAE]^{2+}[TCNE]^{2-}$ are first computed for these isolated systems. The EIM theoretical shielding tensors are then computed and compared to the corresponding experimental principal shifts. The asymmetric unit of the dimer dianions consists of one-half of the $[NEt_4^+]_2[TCNE]_2^{2-}$ molecule[5] and one full $[TDAE]^{2+}[TCNE]_2^{2-}$ molecule.[6] The latter only exhibits near inversion symmetry for the dianion in the $[TDAE]^{2+}$-$[TCNE]_2^{2-}$ lattice. A few comments are appropriate for the icosahedral representation used in this discussion. While the Cartesian representation of shift and shielding tensors is used most frequently to evaluate different molecular orbitals, the icosahedral representation[57] allows for a more reliable procedure for comparing tensors because it preserves the appropriate metric of the problem. The calculated icosahedral nuclear shielding and the experimental icosahedral shift components of these two approaches are compared in Figure 7.

The linear regression equation of this plot has a slope of −1.02 and an intercept of 198 ppm, which compares favorably with the expected slope of −1 and intercept of 188 ppm, respectively. Only modest inconsistencies exist between calculated shieldings with use of the icosahedral[57] and Cartesian methods. The icosahedral distance (a root-mean-squared quantity)[57] between calculated and experimental values is ±4.42 or ±3.82 ppm when the charge array is neglected or included by using EIM, respectively. The quality of the shielding tensors calculated with both methods is comparable to calculations on systems with high symmetry and/or weak lattice effects.[58−61] As the ionic charges are large the high symmetry alternative offers the most likely explanation of the modest differences.

Furthermore, the general gradient approximation in B3LYP may not account for the dynamic electron correlation and

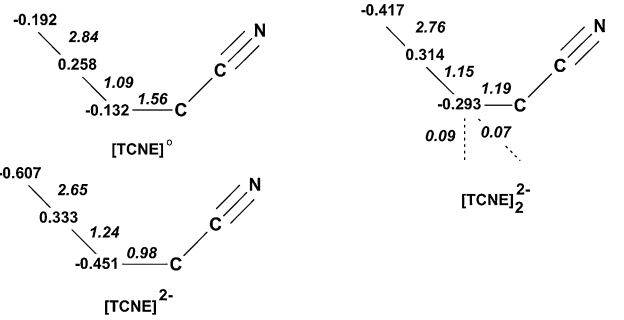

Figure 8. Natural charges and Wiberg bond orders computed for the geometry optimized B3LYP D95** wave functions. The intradimer distance in π-$[TCNE]_2^{2-}$ was set to 2.9 Å. Bond orders are given in italics. Note the charges add to 0, 2−, and 2− for the respective species. Only the unique charges and bond orders are presented and symmetry may be used to determine the other parameters in the isolated molecules and ions.

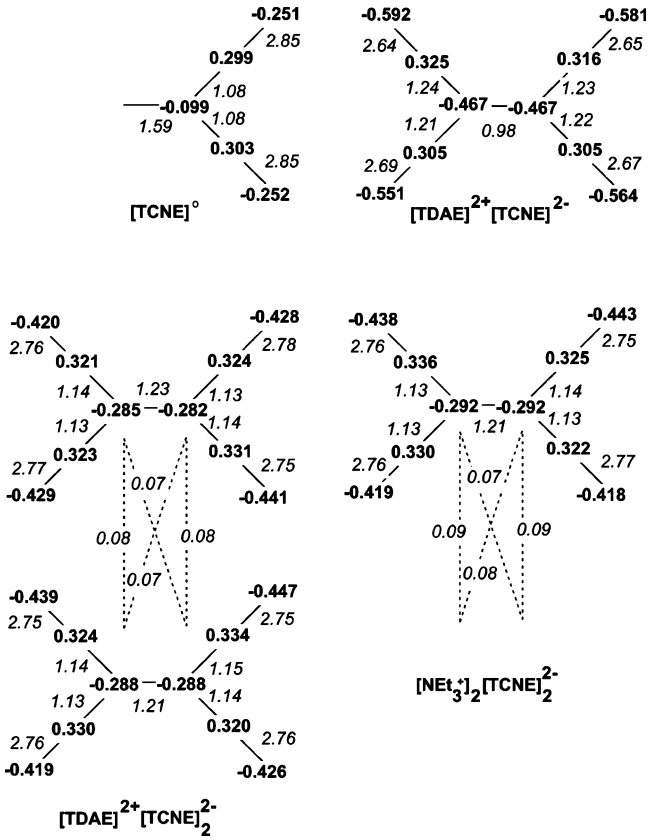

Figure 9. Natural charges and Wiberg bond orders computed for [TCNE], $[TCNE]_2^{2-}$, and $[TCNE]^{2-}$ with the $[NEt_4]^+$ and $[TDAE]^{2+}$ cations, using the EIM B3LYP D95** wave functions. The respective crystal structures were used to generate the point charge arrays and for molecular geometries. Bond orders are given in italics. Only the unique charges and bond orders of the anions in the asymmetric unit are presented.

completely neglects dispersion forces that may be encountered in stacks of $[TCNE]^{\bullet-}$.[62] However, the excellent agreement of experimental shifts with both theoretical shielding models indicates that dispersion forces and stacking effects apparently have only a small perturbation on the calculated shielding values considering the accuracy of the experiment and shielding tensor calculations.

Population Analysis. To interpret the differences in electronic structures among the species examined here, a natural population analysis (NPA) charge and bond-order treatment was performed for the EIM and isolated molecule calculations, respectively.

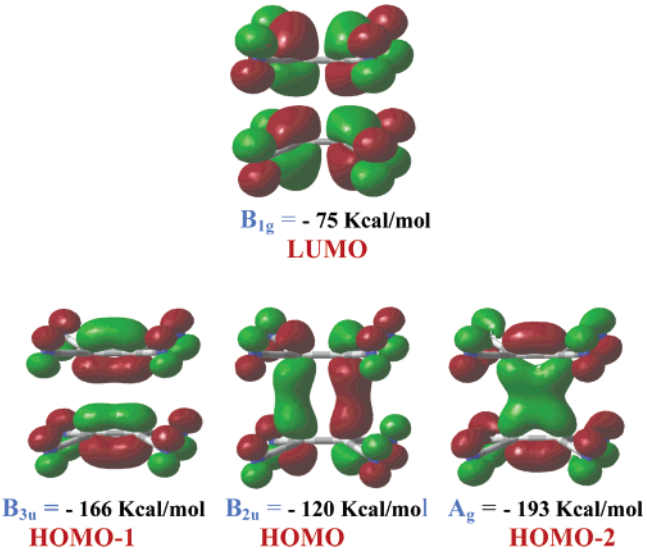

Figure 10. Electron distribution and orbital symmetries are given for the LUMO and the top three HOMOs. In this work the energies for the respective molecular orbitals are reported for B_{1g}, B_{3u}, B_{2u}, and A_g in the EIM-DFT lattice.

We should stress that DFT cannot account for the van der Waals stabilization that earlier theory has shown[2] is needed to compute accurate bond energies in long bonds, thus such a bond-order analysis is likely to underestimate the interanion attractive forces. The theoretical NPA point charges and the Wiberg bond orders in the natural atomic orbital basis (NAO) are given in Figure 8 for the isolated molecules. It is apparent from Figure 8 that the bond order of the central C−C bond decreases upon reduction from 1.56 for TCNE to 0.98 for $[TCNE]^{2-}$. In addition, an increase in $C_{ethylenic}-C_{cyano}$ bond order from 1.09 to 1.24 and a decrease in C≡N bond order from 2.84 to 2.65 are observed, respectively, going from from TCNE° to $[TCNE]^{2-}$. The trends in natural Wiberg bond orders are in accord with the interpretation of the effects observed for the experimental shift components. The bond orders in Figure 8 of the components of the intradimer bond are 0.09 and 0.07, respectively. The sum of these four rather low bond orders accumulates to a significant overall intradimer bond order of 0.32 when all four ethylenic intradimer connections are considered. As noted earlier, this total bond order probably underestimates the strength of the intraanion attraction because the DFT calculations minimize important dispersive van der Waals interactions.[8,9] Furthermore, the negative partial atomic charges on the central ethylenic carbons and on the cyano nitrogen increase upon electronic reduction whereas the positive partial atomic charge on the cyano carbon remains approximately constant.

The theoretical chemical shielding and charge changes are given in Figure 9 for the EIM electrostatic model. Note that the dimer with cations, $[TDEA]^{2+}$, shows a slight break in the symmetry of the theoretical bond orders and charge density as confirmed by a slight break in the inversion symmetry of the chemical shielding values.

LUMO and HOMO Results. As indicated previously, it is usually the LUMO and HOMO that influence the chemical shielding tensors the most because of the close separation of these occupied and unoccupied orbitals and their effect upon the $1/\Delta E$ promotion term of Ramsey.[21] A visual portrayal of the atomic orbital structural arrangements of the MOs and EIM-DFT energies for the B_{1g} LUMO and the three highest occupied MOs [i.e., B_{2u}, B_{3u}, and A_g] are given in Figure 10. The illustration in Figure 10 along with spectroscopic, crystallographic, and NMR results provides an overall consistent description of the π-$[TCNE]_2^{2-}$ dimer. All three HOMOs B_{3u}, B_{2u}, and A_g are responsible for the net intradimer interaction energy. While the B_{3u} orbital has a node perpendicular to the long bond and hence antibonding in character, the A_g and B_{2u} orbitals show sizeable amplitudes between the monomers and both contribute significantly to the bonding of the two ions.

Conclusions

The principal components of the chemical-shift tensors of the ethylenic and cyano carbon positions in TCNE, π-$[TCNE]_2^{2-}$, and $[TCNE]^{2-}$ have been measured in several crystal structures with the FIREMAT experiments. Systematic EIM-DFT shielding tensor calculations allow for the orientation of the principal chemical-shift values in the molecular frame and for a more detailed discussion of the oxidation states of TCNE. The components of the shift tensor of the ethylenic carbon in-plane with the approximate local symmetry reveal a substantial sensitivity to the population of the π^* orbital. This is due to the paramagnetic nuclear shielding that results from mixing ground-state σ and excited-state π^* orbitals in the external magnetic field. The cyano carbon shift tensor components are also affected by oxidation states of TCNE. The most significant effect is observed for the shift tensor component parallel to the CN bond. This is due to the incomplete cancellation of the paramagnetic shielding of the two CN π-bonds. The degree of quenching of the paramagnetic shielding contribution may be related to the $C_{ethylenic}-C_{cyano}$ and the C−N bond orders.

The effect of polarization and electrostatic intermolecular interactions in the molecular ionic crystals on the theoretical ethylenic and cyano shielding tensors is also investigated. Theoretical shielding tensors computed with the EIM method to simulate the surrounding countercation lattice and for the isolated molecules both reveal excellent agreements with the experimentally observed principal shift values. The isolated molecule data are comparable to those obtained with the EIM approach despite the ionic character of the compounds and despite neglect of dispersion forces and exchange due to stacking of π-$[TCNE]_2^{2-}$ dimers with the EIM. The cations apparently provide canceling electrostatic field vectors.

Systematic shielding tensor calculations as a function of intradimer distance in π-$[TCNE]_2^{2-}$ reveal only small shift tensor differences in both the isolated species and EIM-computed ethylenic shielding tensors. These insensitive shielding tensors seem to correlate with the rather flat potential energy curve for the relevant intradimer distance in π-$[TCNE]_2^{2-}$.

Acknowledgment. Helpful discussions with Juan J. Novoa (Barcelona) are gratefully acknowledged. This work was supported by Basic Energy Sciences, U.S. Department of Energy, through grants DE-FG03-94ER14452 and DE-FG03-93ER45504. Computer resources were provided by the Center for High Performance Computing at the University of Utah. We thank Rico Del Sesto, Michelle L. Taliaferro, and Elaine B. Vickers for preparing these samples.

References and Notes

(1) Dixon, D. A.; Miller, J. S. *J. Am. Chem. Soc.* **1987**, *109*, 3656−3664.

(2) Del Sesto, R. E.; Miller, J. S.; Lafuente, P.; Novoa, J. J. *Chem. Eur. J.* **2002**, *8*, 4894−4908 and references therein.

(3) Lü, J.-M.; Rosokha, S. V.; Kochi, J. K. *J. Am. Chem. Soc.* **2003**, *125*, 12161−12171.

(4) Druck, U.; Guth, H. *Z. Kristallog.* **1982**, *161*, 103.

(5) Fox, J. R.; Foxman, B. M.; Guarrera, D.; Miller, J. S.; Calabreses, J. C.; Reis, A. H., Jr. *J. Mater. Chem.* **1996**, *6*, 1627−1631.

(6) Del Sesto, R. E.; Sommer, R. D.; Miller, J. S. *CrystEngComm* **2001**, *47*, 1−3
(7) Johnson, M. T.; Campana, C. F.; Foxman, B. M.; Desmarais, W.; Vela, M. J.; Miller, J. M. *Chem. Eur. J.* **2000**, *6*, 1805−1810.
(8) Jakowski, J.; Simons, J. *J. Am. Chem. Soc.* **2003**, *125*, 16089−16096.
(9) Jung, Y.; Head-Gordon, M. *Phys Chem. Chem. Phys*. **2004**, *6*, 2008−2011.
(10) Pauling, L. *The Nature of the Chemical Bond*, 3rd ed.; Cornell University Press: Ithaca, NY, 1960; p 260.
(11) Cui, Q.; Karplus, M. *J. Phys. Chem. B* **2000**, *104*, 3721−3743.
(12) Bickelhaupt, F. M.; DeKock R. L.; Baerends, E. J. *J. Am. Chem. Soc.* **2002**, *124*, 1500−1505.
(13) *Modeling NMR Chemical-shifts*; Facelli, J. C., De Dios, A. C., Eds.; ACS Symp. Ser., Vol 732; American Chemical Society: Washington, DC, 1999.
(14) Havlin, R.; McMahon, M.; Srinivasan, R.; Le, H.; Oldfield, E. *J. Phys. Chem. A* **1997**, *101*, 8908−8913.
(15) Wallraff, G. M. Disseration, University of Utah, 1985.
(16) Bernard, G. M.; Wasylishen, R. E.; Phillips, A. D. *J. Phys. Chem. A* **2000**, *104*, 8131−8141.
(17) Duncan, T. M. *A Compilation of Chemical-shift Anisotropies*, 2nd ed.; The Farragut Press: Chicago, IL, 1997.
(18) Facelli, J. C.; Grant, D. M. *Theor. Chim. Acta* **1987**, *71*, 277−288.
(19) Beeler, A. J.; Orendt, A. M.; Grant, D. M.; Cutts, P. W.; Michl, J.; Zilm, K. W.; Downing, J. W.; Facelli, J. C.; Schindler, M. S.; Kutzelnigg, W. *J. Am. Chem. Soc.* **1984**, *106*, 7672−7676.
(20) Sherwood, M. H.; Facelli, J. C.; Alderman, D. W.; Grant, D. M. *J. Am. Chem. Soc.* **1991**, *113*, 750.
(21) Ramsey, N. F. *Phys. Rev.*, **1950**, *78*, 699. Ramsey, N. F. *Phys. Rev.* **1952**, *86*, 243.
(22) Maruta, G.; Takeda, S.; Yamaguchi, K.; Ueda, K.; Sugimoto, T. *Synth. Met.* **1999**, *103*, 2333−2334.
(23) Heise, H.; Köhler, F. H.; Herker, M.; Hiller, W. *J. Am. Chem. Soc.* **2002**, *124*, 10823−10832.
(24) Iuliucci, R. J.; Facelli, J. C.; Alderman, D. W.; Grant, D. M. *J. Am. Chem. Soc.* **1995**, *117*, 2336−2343.
(25) Strohmeier, M.; Grant, D. M. *J. Am. Chem. Soc.* **2004**, *126*, 966−977.
(26) Augspurger, J.; Pearson, J. G.; Oldfield, E.; Dykstra, C. E.; Park, K. D.; Schwartz, D. *J. Magn. Reson.* **1992**, *100*, 342−357.
(27) Asakawa, N.; Kuroki, S.; Kurosu, H.; Ando, I.; Shoji, A.; Ozaki, T. *J. Am. Chem. Soc.* **1992**, *114*, 3261−3265.
(28) Gu, Z.; Zambrano, R.; McDermott, A. *J. Am. Chem. Soc.* **1994**, *116*, 6368−6372.
(29) Soderquist, A.; Facelli, J. C.; Horton, W. J.; Grant, D. M. *J. Am. Chem. Soc.* **1995**, *117*, 8441−8446.
(30) Harper, J. K.; McGeorge, G.; Grant, D M. *J. Am. Chem. Soc.* **1999**, *121*, 6488−6496.
(31) Bax, A. *J. Magn. Reson.* **1985**, *65*, 142−145.
(32) White, J. L.; Beck, L. W.; Ferguson, D. B.; Haw, J. F. *J. Magn. Reson.* **1992**, *100*, 336−341.
(33) Dixon, W. T.; Schaefer, J.; Sefcik, M. D.; Stejskal, E. O.; McKay, R. A. *J. Magn. Reson.* **1982**, *49*, 341−345.
(34) Alderman, D. W.; McGeorge, G.; Hu, J. Z.; Pugmire, R. J.; Grant, D. M. *Mol. Phys.* **1998**, *95*, 1113−1126.
(35) McGeorge, G.; Hu, J. Z.; Mayne, C. L.; Alderman, D. W.; Pugmire, R. J.; Grant, D. M. *J. Magn. Reson.* **1997**, *129*, 134−144.
(36) Strohmeier, M.; Alderman, D. W.; Grant, D. M. *J. Magn. Reson.* **2002**, *155*, 263−277.
(37) Frisch, M. J.; Trucks, G. W.; Schlegel, H. B. et al. *Gaussian 98* and *Gaussian 03*; Gaussian, Inc.; Pittsburgh, PA, 1998 and 2003.
(38) London, F. *J. Phys. Radium* **1937**, *8*, 397.
(39) Wolinski, K.; Hinton, J. F.; Pulay, P. *J. Am. Chem. Soc.* **1990**, *112*, 8251−8260.
(40) Becke, A. D. *J. Chem. Phys.* **1993**, *98*, 5648−5652.
(41) Lee, C.; Yang, W.; Parr, R. G. *Phys. Rev. B* **1988**, *37*, 785−789.
(42) Dunning, T. H., Jr. *J. Chem. Phys.* **1989**, *90*, 1007−1023.
(43) Cheeseman, J. R.; Trucks, G. W.; Keith, T. A.; Frisch, M. J. *J. Chem. Phys.* **1996**, *104*, 5497−5509.
(44) *NBO*, Version 3.1; Glendening, E. D., Reed, A. E., Carpenter, J. E., Weinhold, F.
(45) Grant, D. M. In *Encyclopedia of NMR*; Grant, D. M., Harris, R. K., Eds.; John Wiley: Chichester, UK, 1996; Vol. 2, pp 1298−1312.
(46) Facelli, J. C.; Grant, D. M. In *Topics in Stereochemistry*; Eliel, E. L., Wilen, S. H., Eds.; John Wiley & Sons: New York, 1989; Vol. 19, pp 1−61.
(47) Pines, A.; Kaplan, S.; Griffin, R. G.; Waugh, J. S. *Chem. Phys. Lett.* **1974**, *25*, 78.
(48) Wiberg, K. B.; Hammer, J. D.; Zilm, K. W.; Keith, T. A.; Cheeseman, J. R.; Duchamp, J. C. *J. Org. Chem.* **2004**, *69*, 1086−1096.
(49) Stueber, D.; Guenneau, F. N.; Grant, D. M. *J. Chem. Phys.* **2001**, *114*, 9236−9243.
(50) Reed, A. E.; Weinhold, F. *J. Chem. Phys.* **1983**, *78*, 4066−4073.
(51) Reed, A. E.; Weinstock, R. B.; Weinhold, F. *J. Chem. Phys.* **1985**, *83*, 735−746.
(52) Ewald, P. P. *Ann. Phys*. **1921**, *64*, 253−287.
(53) Stueber, D.; Patterson, D.; Mayne, C. L.; Orendt, A. M.; Grant, D. M.; Parry, R. W. *Inorg. Chem.* **2001**, *40*, 1902−1911.
(54) Stueber, D.; Arif, A. M.; Grant, D. M.; Parry, R. W. *Inorg. Chem.* **2001**, *40*, 1912−1914.
(55) Stueber, D.; Orendt, A. M.; Facelli, J. C.; Parry, R. W.; Grant, D. M. *Solid State NMR* **2002**, *22*, 29−49.
(56) Strohmeier, M.; Stueber, D.; Grant, D. M. *J. Phys. Chem. A* **2003**, *107*, 7629−7642.
(57) Alderman, D. W.; Sherwood, M. H.; Grant, D. M. *J. Magn. Reson.* **1993**, *101*, 188−197.
(58) Barich, D. H.; Hu, J. Z.; Pugmire, R. J.; Grant, D. M. *J. Phys. Chem. A* **2002**, *106*, 6477−6482.
(59) Barich, D. H.; Facelli, J. C.; Hu, J. Z.; Alderman, D. W.; Wang, W.; Pugmire, R. J.; Grant, D. M. *Magn. Reson. Chem*. **2001**, *39*, 115−121.
(60) Orendt, A. M.; Facelli, J. C.; Bai, S.; Rai, A.; Gossett, M.; Scott, L. T.; Boerio-Goates, J.; Pugmire, R. J.; Grant, D. M. *J. Phys. Chem. A* **2000**, *104*, 149−155.
(61) Barich, D. H.; Orendt, A. M.; Pugmire, R. J.; Grant, D. M. *J. Phys. Chem. A* **2000**, *104*, 8290−8295.
(62) Kristian, S.; Pulay, P. *Chem. Phys. Lett.* **1994**, *229*, 175.